

[¹⁸F]F-AraG Uptake in Vertebral Bone Marrow May Predict Survival in Patients with Non–Small Cell Lung Cancer Treated with Anti-PD-(L)1 Immunotherapy

Jelena Levi¹, Millie Das^{2,3}, Minal S. Vasanaawala^{2,3}, Deepti Behl⁴, Martin Pomper⁵, Patrick M. Forde⁵, Erica Nakajima⁵, James Sayre⁶, Bin Shen^{†7}, Hilda Cabrera¹, Niko Del Mar², Michele Gullen⁴, Michele Pierini⁴, Laura Cox⁴, Ojaswita Lokre⁸, Timothy Perk⁸, and Hee-Don Chae¹

¹CellSight Technologies Inc., San Francisco, California; ²Department of Medicine, Stanford University, Palo Alto, California; ³Veterans Affairs Palo Alto Health Care System, Palo Alto, California; ⁴Sutter Medical Center, Sacramento, California; ⁵Johns Hopkins Kimmel Cancer Center, Baltimore, Maryland; ⁶Department of Radiology, David Geffen School of Medicine at UCLA, UCLA Center for the Health Sciences, Los Angeles, California; ⁷Department of Radiology, Stanford University, Palo Alto, California; and ⁸AIQ Solutions, Madison, Wisconsin

Despite the systemic impact of both cancer and the associated immune response, immuno-PET is predominantly centered on assessment of the immune milieu within the tumor microenvironment. The aim of this study was to assess the value of [¹⁸F]F-AraG PET imaging as a noninvasive method for evaluation of system-wide immune status of patients with non–small cell lung cancer before starting immunotherapy. **Methods:** Eleven patients with advanced non–small cell lung cancer were imaged with [¹⁸F]F-AraG before starting immunotherapy. Diagnostic [¹⁸F]FDG PET/CT scans were analyzed to assess differences in the extent of disease among patients. SUV_{max}, SUV_{mean}, and total SUV (SUV_{total}) from all tumor lesions, active lymph nodes, spleen, vertebral bone marrow, liver, thyroid, heart, and bowel were extracted from the baseline [¹⁸F]F-AraG scans, and discriminant and Kaplan–Meier analyses were performed to test their ability to predict patient response and overall survival. **Results:** The extent of the disease was variable in the patient cohort, but none of the [¹⁸F]FDG biomarkers associated with tumor burden (SUV_{max}, total metabolic tumor volume, and total lesion glycolysis) was predictive of patient survival. The differences in the [¹⁸F]F-AraG and [¹⁸F]FDG distribution were observed both within and between lesions, confirming that they capture distinct aspects of the tumor microenvironment. Of the 3 SUV parameters studied, [¹⁸F]F-AraG SUV_{total} provided a dynamic range suitable for stratifying tumors or patients according to their immune activity. [¹⁸F]F-AraG SUV_{total} measured in the lumbar and sacral vertebrae differentiated between patients who progressed on therapy and those who did not with 90.9% and 81.8% accuracy, respectively. The Kaplan–Meier analysis revealed that patients with high [¹⁸F]F-AraG SUV_{total} in the lumbar bone marrow had significantly lower probability of survival than those with a low signal ($P = 0.0003$). **Conclusion:** This study highlights the significance of assessing systemic immunity and indicates the potential of the [¹⁸F]F-AraG bone marrow signal as a predictive imaging biomarker for patient stratification and treatment guidance.

Key Words: molecular imaging, oncology, non–small cell lung cancer, systemic immunity

J Nucl Med 2024; 00:1–7

DOI: 10.2967/jnumed.124.268253

Received Jun. 16, 2024; revision accepted Sep. 25, 2024.

For correspondence or reprints, contact Jelena Levi (jlevi@cellsighttech.com).

[†]Deceased.

Published online Oct. 24, 2024.

COPYRIGHT © 2024 by the Society of Nuclear Medicine and Molecular Imaging.

Lung cancer is the leading cause of cancer-related mortality in both women and men worldwide. Approximately 85% of lung cancers are classified as non–small cell lung cancer (NSCLC), a heterogeneous group of diseases with diverse molecular features and pathology (1). Immunotherapy has emerged as a breakthrough treatment for patients without driver mutations, becoming a fundamental element in the treatment of advanced disease. Immune checkpoint inhibitors, monoclonal antibodies directed at immune checkpoints, such as programmed death-1 (PD-1), or its ligand PD-L1, disrupt immune tolerance to cancer and enable effective and durable anti-tumor responses that lead to improved overall survival (2,3). Unfortunately, many patients do not benefit from the treatment, and identifying patients who will most likely respond to checkpoint inhibitors remains a difficult clinical challenge. The most extensively studied biomarkers of response rely on invasive biopsies and are confined to assessment only within the tumor microenvironment; they include PD-L1 expression, tumor mutational burden, and tumor-infiltrating lymphocytes. However, because of the inherent limitations of biopsy, those biomarkers cannot adequately capture heterogeneity of the immune contexture, both within a tumor lesion and between different lesions in patients with extensive disease (4). Furthermore, historical knowledge (5) and recent discoveries (6,7) underscore the significance of the global immune context and urge a shift away from exclusive focus on the tumor microenvironment and local immune aspects.

The capacity of PET to noninvasively monitor processes on a whole-body level makes it a particularly well-suited method for assessing system-wide immune status. Several PET tracers, differing in size and what they assess, are currently being investigated as biomarkers for immune profiling and assessment of immunotherapy response (8,9). Radiotracers that target immune activation, such as those assessing activation pathways (10) or markers such as CD69 (11) and OX40 (12), offer the ability to evaluate not only the presence but also the functional state of key players in adaptive antitumoral immune response. Small-molecule metabolic radiotracers are particularly appealing in this context, as their size facilitates effective penetration through biologic barriers and assessment of target distribution throughout the body (13). [¹⁸F]F-AraG is a small-molecule mitochondrial metabolic tracer that tracks activated T cells by assessing metabolic reprogramming associated with their

function (14). Preclinically, [¹⁸F]F-AraG has shown utility in the evaluation of immunotherapy response (15) and also in immune profiling before initiating therapy (16). Characterization of pretreatment immune status and its correlation with response to therapy and clinical outcome are of critical importance in understanding the value of [¹⁸F]F-AraG PET in patient selection. In this study, we examine the systemic immune status of patients with NSCLC using pretreatment [¹⁸F]F-AraG scans and demonstrate that [¹⁸F]F-AraG uptake in vertebral bone marrow can predict clinical outcome.

MATERIALS AND METHODS

Study Participants and Clinical Trials

This study included patients enrolled in a clinical trial aimed at imaging T cell activation in patients with advanced NSCLC (NCT04726215). Participants were enrolled at 2 institutions: Palo Alto Veterans Affairs (5 patients) and Sutter Medical Center in Sacramento (6 patients). The studies were approved by the Stanford University panel on human subjects in medical research and the Sutter Health Institutional review board, and all participants signed a written informed consent form. Standard of care, diagnostic, [¹⁸F]FDG scans were also collected. The response to therapy was defined according to RECIST criteria (for patients at Sutter Medical Center) and based on the treating oncologist's discretion (for patients at Palo Alto Veterans Affairs).

[¹⁸F]F-AraG PET/CT Imaging

[¹⁸F]F-AraG PET/CT imaging was performed at the institution where participants were enrolled following the same imaging protocol. Patients received a bolus venous injection of 185 MBq ($\pm 10\%$) of [¹⁸F]F-AraG, followed by whole-body imaging at approximately 60 min after injection. The GE Discovery MI and GE Discovery STE scanners were used at Palo Alto Veterans Affairs, whereas a Siemens Biograph 40 mCT was used at Sutter Medical Center. Images were reconstructed using iterative algorithms and using CT for attenuation correction. The following image reconstruction parameters were used: 3-dimensional (3D) infrared (3D ordered-subset expectation maximization) with time of flight on, 8 subsets, 3 iterations, and a 6.0-mm filter cutoff; no z-axis filter (GE Discovery MI); 3D infrared (3D ordered-subset expectation maximization) with no time of flight, 20 subsets, 2 iterations, and a 6.0-mm filter cutoff; no z-axis filter (GE Discovery STE) and TrueX with time of flight (ultra-high-definition PET) reconstruction, 2 iterations, 21 subsets, gaussian filter with a full width at half maximum of 2.0 mm (Siemens Biograph).

Image Analysis

All individual [¹⁸F]FDG and [¹⁸F]F-AraG PET/CT scans were analyzed using TRAQinform IQ (AIQ Solutions), a software-only medical device intended for use by trained medical professionals. A nuclear medicine physician manually identified regions of interest (ROI), which included lesions on [¹⁸F]FDG PET/CT images, and hot spots, with PET uptake elevated from the background, on [¹⁸F]F-AraG PET/CT images. [¹⁸F]F-AraG hot-spot contours were generated independently of [¹⁸F]FDG contours by referencing both CT and PET images. If the local SUV was significantly higher than that of the surrounding tissue or similar parts of the normal image, the ROI was included. Additionally, the ROIs were included if there was an abnormal presentation on the CT images. Automated organ contours were manually reviewed and corrected for motion and spillover. The TRAQinform IQ software performed automated matching of ROI across the [¹⁸F]FDG and [¹⁸F]F-AraG images (17–20) and performed quantitative analysis of ROI on the PET/CT images. Moreover, the software also performed automatic organ segmentation, trained using the method outlined in Weisman et al., to provide quantification and locations of lesion ROI (21).

From every PET/CT image, TRAQinform IQ software extracted single time-point image features from the scans in each individual

ROI: SUV_{max} (the highest SUV within the ROI), SUV_{mean} (the average SUV in the ROI), volume (the total volume of the ROI, which for [¹⁸F]FDG is equivalent to metabolic tumor volume [MTV]), and SUV_{total} (the total SUV in the ROI, which for [¹⁸F]FDG is equivalent to total lesion glycolysis [TLG]). SUV_{max}, SUV_{mean}, SUV_{total}, and SUV volume were extracted for the liver, spleen, thyroid, bowel, heart, and spine.

Statistical Analysis

Means, medians, and SD of each quantitative variable and percentages for qualitative variables were computed. Kolmogorov–Smirnov tests were computed to assess normal distribution assumptions. The ability of the [¹⁸F]FDG and [¹⁸F]F-AraG measures for various patient organ and skeletal elements to distinguish between progressive disease and nonprogressive disease was investigated by a stepwise multivariate

TABLE 1
Patient Characteristics

Characteristic	Patient cohort
Median age (y)	72 (range, 55–81)
Sex	
Female	3 (27)
Male	8 (73)
PET Center	
Palo Alto Veterans Affairs	5 (45.6)
Sutter Health at Sacramento	6 (54.6)
Race	
Black	1 (9.1)
Asian	1 (9.1)
White	7 (63.6)
Unknown	2 (18.2)
ECOG performance status	
0	3 (27.3)
1	6 (54.5)
2	2 (18.2)
Tumor stage	
IV	11 (100)
Therapy	
Pembrolizumab	10 (66.7)
Atezolizumab	1 (6.6)
Metastatic site	
Liver	2 (13)
Brain	0 (0)
Bone marrow	7 (47)
Adrenal	5 (33)
Lymph node	3 (20)
PD-L1	
1%–50%	3
>50%	2
Unknown	6

Qualitative data are number and percentage.
ECOG = Eastern Cooperative Oncology Group.

discriminant analysis. The aim of this analysis was to obtain measures that would yield the largest total correct classification percentage. The cutoff point for this discriminant analysis was then used by the univariate survival analysis using Kaplan–Meier plots and Mantel–Cox tests. All these analyses were performed using IBM SPSS Statistics for Windows, version 28.0. As a further validation of the cut point, a classification and regression tree analysis was performed using Minitab version 21.4.1 (Minitab LLC).

RESULTS

Patient Demographics

Eleven patients with advanced NSCLC were enrolled and imaged at 2 institutions: Palo Alto Veterans Affairs (5 patients) and Sutter Medical Center in Sacramento (6 patients) (Table 1). The cohort included 8 men and 3 women; all patients had stage IV disease. Two patients had liver metastasis, and no patient had brain metastasis. One patient received atezolizumab (a PD-L1 inhibitor), and 10 patients were treated with pembrolizumab (a PD-1 inhibitor). PD-L1 status was known for 5 patients (46%). The patients were followed for 12 mo, during which time 3 patients (27%) died. Four patients (36%) developed progressive disease, 5 patients (46%) had a partial response, 1 patient (9%) had stable disease, and 1 patient (9%) had a complete response.

[¹⁸F]FDG Biomarkers Were Not Predictive of Survival in Patients with Metastatic NSCLC

As tumor burden affects patients' responses to therapy (22), we analyzed baseline diagnostic [¹⁸F]FDG PET/CT scans to assess the differences in the extent of disease among patients. Diagnostic [¹⁸F]FDG PET/CT scans were available for all patients and were acquired 16–56 d (median, 36 d) before the [¹⁸F]F-AraG scan. We analyzed the SUVs most commonly associated with tumor burden: SUV_{max}, total metabolic tumor volume (tMTV), and TLG. The extent of the disease differed between patients (Fig. 1A). In the

patient cohort, SUV_{max} ranged from 5.2 to 44.5, tMTV spanned from 27.8 to 790.5 cm³, and TLG ranged from 70.8 to 3,531.4. The Kaplan–Meier analysis did not show significant differences in the probability of survival between patients with different TLG (cutoff, 1,654.3; *P* = 0.40) or tMTV (cutoff, 362.6 cm³; *P* = 0.11) (Figs. 1B and 1C). Moreover, no significant differences in SUV_{max} were noted between patients who progressed on therapy and those who did not (Supplemental Fig. 1; supplemental material is available at <http://jnm.snmjournals.org>).

[¹⁸F]FDG and [¹⁸F]F-AraG Have Different Inter- and Intralesional Uptake Distribution

Our preclinical studies have shown that [¹⁸F]F-AraG, unlike [¹⁸F]FDG, selectively accumulates in activated T lymphocytes over tumor cells, providing information on immune contexture within the tumor microenvironment (15). In this patient cohort, differences between [¹⁸F]FDG and [¹⁸F]F-AraG uptake (Supplemental Table 1) were noted across various lesions within the same patient (Fig. 2A), as well as within the same lesion (Fig. 2B), capturing distinct aspects of the tumor microenvironment. Similar to what was observed in the preclinical studies (16), [¹⁸F]F-AraG's intralesional distribution patterns resembled discrete cancer-immune phenotypes: inflamed, immune excluded, and immune desert (Fig. 2B). The observed differences between [¹⁸F]FDG and [¹⁸F]F-AraG, as well as [¹⁸F]F-AraG's pattern of lesional uptake, indicate that within tumors [¹⁸F]F-AraG does not accumulate in cancer cells (15,23).

[¹⁸F]F-AraG SUV_{total} Offers a Dynamic Range Needed for Stratification of Immune Activity

SUVs are commonly used for quantitative assessment of [¹⁸F]FDG uptake. To understand the use of SUV measurements in the context of [¹⁸F]F-AraG and assessment of immune status, we extracted different parameters, SUV_{max}, SUV_{mean}, and SUV_{total}, and determined the extent of their variation within the patient cohort. The median maximum value for all 3 SUV parameters was considerably lower for [¹⁸F]F-AraG than for [¹⁸F]FDG (Table 2; Supplemental Table 2). The range of values for these parameters was also notably narrower for [¹⁸F]F-AraG than for [¹⁸F]FDG. Expectedly, the narrower range was observed for SUV_{mean}, whereas SUV_{total} displayed the widest range. Although [¹⁸F]F-AraG SUV_{total} provides a dynamic range essential for stratifying tumors or patients according to their immune activity, it is important to acknowledge that the variability in SUV_{total} stems primarily from differences in lesion volume. Given its dependence on lesion size, [¹⁸F]F-AraG SUV_{total} is most reliable for comparisons within lesions of similar sizes or among patients with comparable tumor burdens.

[¹⁸F]F-AraG Uptake in the Vertebral Bone Marrow Identifies Patients with Progressive Disease

As cancer, a metastatic disease in particular, represents a complex systemic condition that affects immunity as well as distant organs (24), we assessed [¹⁸F]F-AraG accumulation in the spleen, vertebral bone marrow, liver, thyroid, heart, and bowel.

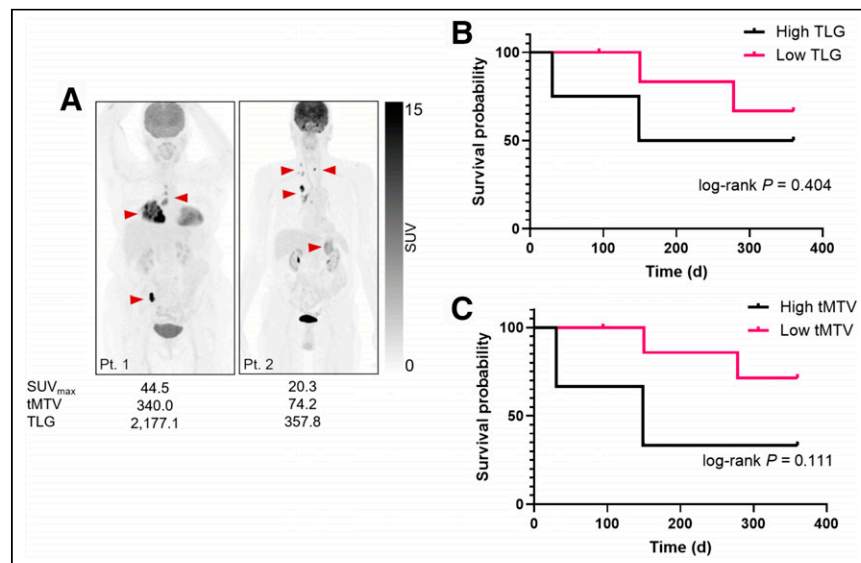


FIGURE 1. Tumor burden and overall survival. (A) Diagnostic [¹⁸F]FDG scan was used to assess extent of disease. Tumor burden differed greatly between patients. (B) Kaplan–Meier analysis did not show statistically significant difference in probability of survival between patients with different TLG (cutoff, 1,654.3). (C) Kaplan–Meier analysis did not show statistically significant difference in probability of survival between patients with different tMTV (cutoff, 362.6 cm³). Pt. = patient.

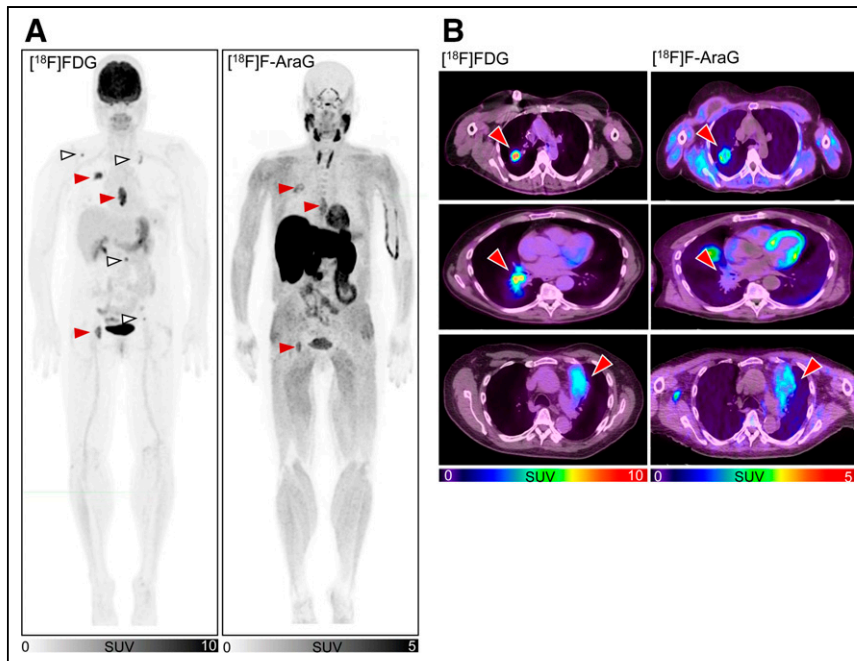


FIGURE 2. Inter- and intralesional differences between $[^{18}\text{F}]\text{FDG}$ and $[^{18}\text{F}]\text{F-AraG}$. (A) Representative $[^{18}\text{F}]\text{FDG}$ and $[^{18}\text{F}]\text{F-AraG}$ patient images. $[^{18}\text{F}]\text{F-AraG}$ uptake differed between $[^{18}\text{F}]\text{FDG}$ -avid lesions. $[^{18}\text{F}]\text{F-AraG}$ accumulated in some (red arrowheads) but not all (white arrowheads) lesions. (B) Representative $[^{18}\text{F}]\text{FDG}$ and $[^{18}\text{F}]\text{F-AraG}$ transaxial slices showing lung lesion (arrowhead) in 3 patients. Intralesional signal distribution differed between $[^{18}\text{F}]\text{FDG}$ and $[^{18}\text{F}]\text{F-AraG}$. $[^{18}\text{F}]\text{F-AraG}$ signal distribution resembles distribution of immune infiltrates in common cancer-immune phenotypes: immune excluded (immune cells on tumor margins, top row), immune desert (very few immune cells, middle row), and inflamed (immune cells in tumor core, bottom row).

$[^{18}\text{F}]\text{F-AraG}$ uptake in those organs differed greatly between patients (Fig. 3A; Supplemental Table 3). To comprehensively evaluate systemic immunity, we performed discriminant analysis using SUVs extracted from these organs along with those from all tumor lesions and active lymph nodes (Supplemental Table 4). $[^{18}\text{F}]\text{F-AraG}$ $\text{SUV}_{\text{total}}$ measured in the lumbar (Fig. 3B) and sacral vertebrae (Supplemental Fig. 2) differentiated between patients who progressed on therapy from those who did not with 90.9% and 81.8% accuracy, respectively. That stands in contrast to $[^{18}\text{F}]\text{FDG}$ $\text{SUV}_{\text{total}}$ measured in the vertebral bone marrow, which showed no significant distinctions ($P = 0.44$) between these 2 groups (Fig. 3C). $[^{18}\text{F}]\text{F-AraG}$ $\text{SUV}_{\text{total}}$ measured in the cervical and thoracic bone marrow did not differ significantly between patients who had progressive disease and those who did not (Supplemental Fig. 2). The volume of vertebral ROIs was not different between patients with progressive and those with nonprogressive disease, indicating that the findings for lumbar and sacral $[^{18}\text{F}]\text{F-AraG}$

TABLE 2
SUVs Detected for $[^{18}\text{F}]\text{FDG}$ and $[^{18}\text{F}]\text{F-AraG}$ in Lesions

Parameter	SUV_{max}	SUV_{mean}	$\text{SUV}_{\text{total}}$
$[^{18}\text{F}]\text{FDG}$			
Median maximum	14.3	3.4	713.2
Range	5.2–44.5	2.1–6.2	70.8–3,531.4
$[^{18}\text{F}]\text{F-AraG}$			
Median maximum	4.2	1.7	111.7
Range	3–5.7	1.1–3.6	16.4–1,333.5

$\text{SUV}_{\text{total}}$ were independent of volume effects (Supplemental Table 5).

$[^{18}\text{F}]\text{F-AraG}$ $\text{SUV}_{\text{total}}$ in Lumbar Bone Marrow Predicts Overall Survival

The discriminant analysis identified an optimal cutoff value of 485.9 for lumbar $[^{18}\text{F}]\text{F-AraG}$ $\text{SUV}_{\text{total}}$, which stratified patients into high and low signal groups. The Kaplan–Meier analysis revealed that patients with high $[^{18}\text{F}]\text{F-AraG}$ $\text{SUV}_{\text{total}}$ in the lumbar bone marrow had a significantly lower probability of survival than those with a low signal (Fig. 4A). Notably, 2 patients with comparable tumor burden as assessed by $[^{18}\text{F}]\text{FDG}$ and similar immune tumor microenvironment as determined by intralesional $[^{18}\text{F}]\text{F-AraG}$, but with contrasting lumbar bone marrow $[^{18}\text{F}]\text{F-AraG}$ $\text{SUV}_{\text{total}}$, exhibited distinct clinical outcomes (Fig. 4; Supplemental Fig. 3). These results suggest that the $[^{18}\text{F}]\text{F-AraG}$ signal in the vertebral bone marrow could serve as a predictive biomarker of patient outcome. Further investigation is warranted to elucidate biologic mechanisms underlying the observed survival disparities.

DISCUSSION

Cancer is a systemic disease that affects the entire organism, including the immune terrain. Despite the systemic impact of both cancer and the associated immune response, tumor immunology is predominantly centered on the immune milieu within the tumor microenvironment. There is an urgent need for a more comprehensive understanding of the organismic immune context. In this study, we investigated $[^{18}\text{F}]\text{F-AraG}$ PET imaging as a noninvasive method for assessment of system-wide immune status of patients with advanced NSCLC before starting immunotherapy. We extracted potential $[^{18}\text{F}]\text{F-AraG}$ biomarkers from patients' baseline scans and tested their ability to predict patient response and overall survival.

The patient cohort studied was heterogeneous, displaying large variations in the extent of the disease. As disease load affects immunity and response to immunotherapy (25), we first examined the value of $[^{18}\text{F}]\text{FDG}$ biomarkers associated with tumor burden in predicting patient overall survival. None of the analyzed $[^{18}\text{F}]\text{FDG}$ biomarkers, SUV_{max} , tMTV , and TLG , correlated with overall survival. Studies that investigated the predictive value of baseline $[^{18}\text{F}]\text{FDG}$ biomarkers in immunotherapy-treated patients with NSCLC have reported conflicting findings. Although Evangelista et al. did not observe significant differences in the whole-body TLG and MTV between responders and nonresponders (26), other studies reported an association between higher MTV and poor overall survival (27,28). The inconsistent findings could stem from the differences in how lesions are segmented, as well as the variations in patient characteristics across the studies. In our study, the expression of PD-L1, a biomarker of response to anti-PD-1 therapy, was unknown for more than half of the patients, and at least 3 patients had an expression level below the threshold linked with a favorable response to therapy. This may explain discrepancies with studies reporting the predictive value of tMTV and TLG , which included only patients

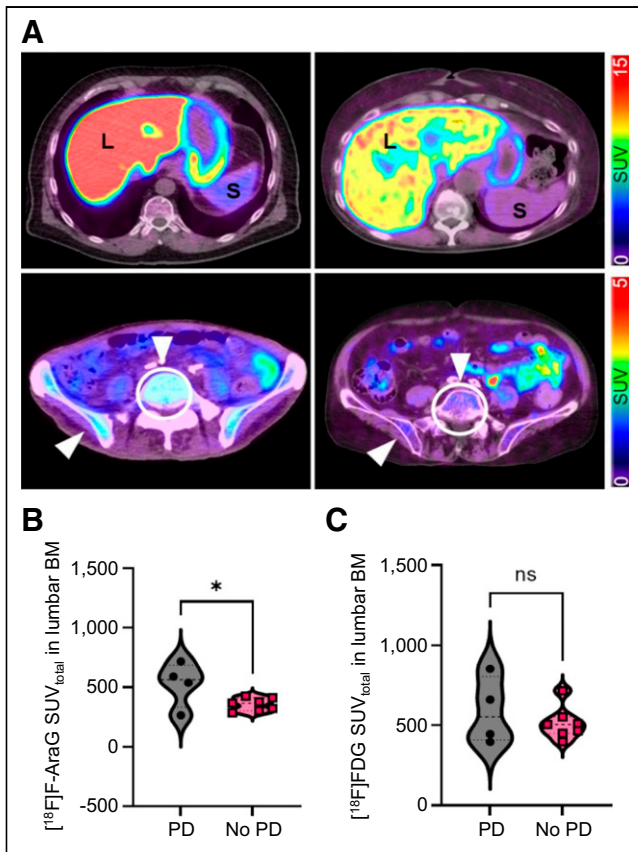


FIGURE 3. $[^{18}\text{F}]\text{F-AraG}$ accumulation in lymphoid organs. (A) Accumulation in lymphoid and nonlymphoid organs differed between patients; white arrowheads point to bone marrow in lumbar vertebrae and iliac bone. (B) $[^{18}\text{F}]\text{F-AraG}$ $\text{SUV}_{\text{total}}$ in lumbar bone marrow differed significantly between patients with progressive disease and those without ($P = 0.046$). (C) $[^{18}\text{F}]\text{FDG}$ $\text{SUV}_{\text{total}}$ in lumbar bone marrow did not differ significantly between patients who had progressive disease and those who did not ($P = 0.44$). L = liver; S = spleen; BM = bone marrow; PD = progressive disease; ns = not significant.

with high PD-L1 expression (>50%). However, our findings remain clinically relevant as immunotherapy commonly extends to patients with lower PD-L1 expression (<50%).

The overlap in metabolic needs between cancer cells and activated immune cells leads to $[^{18}\text{F}]\text{FDG}$ accumulation in both, rendering $[^{18}\text{F}]\text{FDG}$ a nonspecific tracer for immune cells (29). In contrast to $[^{18}\text{F}]\text{FDG}$ and because of the intricate regulation of nucleotide pools and mitochondrial biogenesis in T cells (14), $[^{18}\text{F}]\text{F-AraG}$ has shown preferential accumulation in activated T lymphocytes. We observed differences in the distribution of these 2 tracers, both within and between lesions, which aligned with our expectations considering their respective targets. In contrast to $[^{18}\text{F}]\text{FDG}$, which primarily indicates metabolically active cancer cells, the uptake patterns of $[^{18}\text{F}]\text{F-AraG}$ within tumor lesions resembled distinct immune landscapes observed clinically. The level of intralesional $[^{18}\text{F}]\text{FDG}$ uptake exceeded that of $[^{18}\text{F}]\text{F-AraG}$, an expected finding considering the differences in the number of cancer and immune cells present within a lesion, as well as the level of glycolysis in relation to mitochondrial biogenesis (30). In addition, the range of the values for the 3 metrics tested was

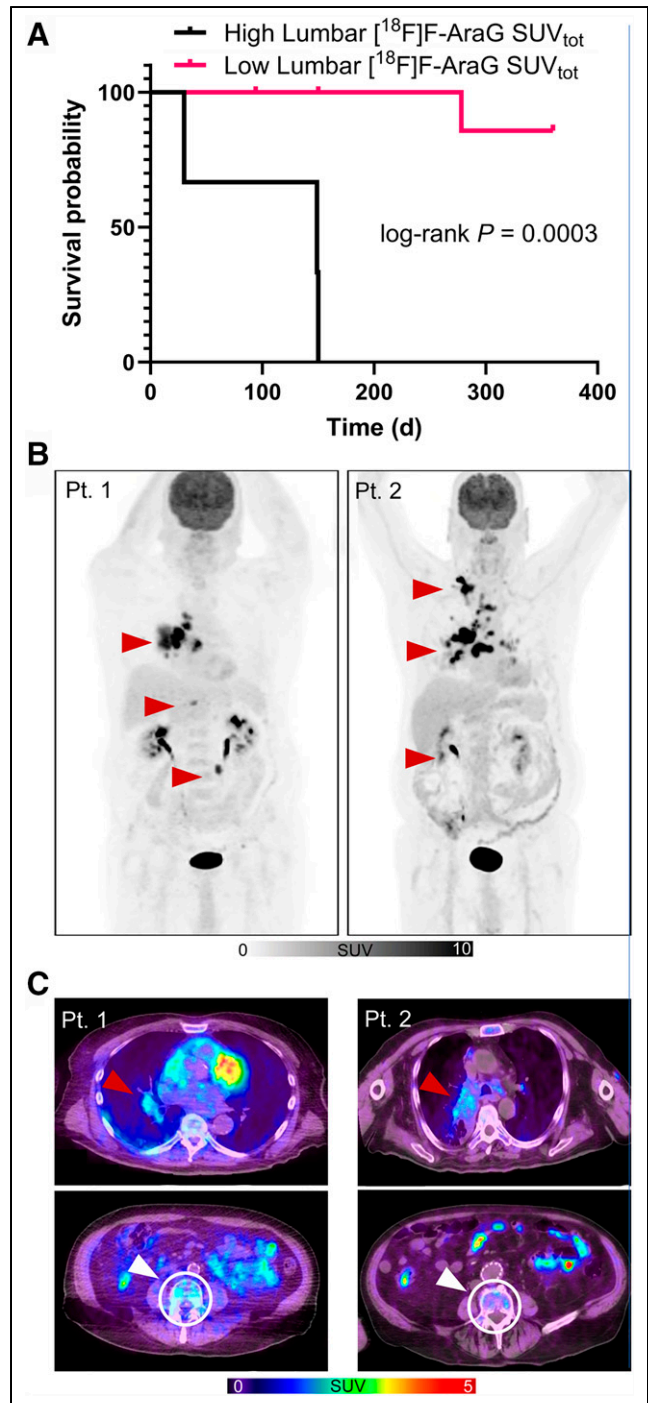


FIGURE 4. High $[^{18}\text{F}]\text{F-AraG}$ uptake in lumbar bone marrow correlates with decreased overall survival. (A) Kaplan–Meier analysis revealed significantly lower probability of survival in patients with high accumulation of $[^{18}\text{F}]\text{F-AraG}$ in lumbar bone marrow. (B) Tumor burden in 2 patients with different clinical outcomes. Patient 1 (TLG, 1,800) had progressive disease and died less than 5 mo after starting therapy. Patient 2 (TLG, 2,162) had complete response and was alive at time of analysis, more than 12 mo after start of therapy. (C) Lung lesion in 2 patients showed comparable $[^{18}\text{F}]\text{F-AraG}$ accumulation (top row). $[^{18}\text{F}]\text{F-AraG}$ accumulation in bone marrow lumbar 4 vertebrae of patient with shorter survival was considerably higher than uptake in patient with longer survival. Pt. = patient.

considerably lower for [¹⁸F]F-AraG than for [¹⁸F]FDG. The limited variability observed in [¹⁸F]F-AraG SUV_{max} across patients suggests that the highest image pixel intensity within the volume of interest may not be a suitable metric for accurate classification of immunologic activity within the tumor microenvironment. [¹⁸F]F-AraG SUV_{mean}, indicative of average immune activity, also exhibited minimal variation between patients, whereas [¹⁸F]F-AraG SUV_{total}, representing total immune activity, demonstrated a wider range of values across the patient cohort.

Interestingly, our study revealed substantial variability in the [¹⁸F]F-AraG SUV_{total} within the lymphoid organs across patients. Although studies suggest the importance of the [¹⁸F]FDG signal in the spleen in immunotherapy response (31), in this patient cohort, neither [¹⁸F]FDG nor [¹⁸F]F-AraG SUVs in the spleen showed significant differences between responders and nonresponders (Supplemental Fig. 4). However, [¹⁸F]F-AraG SUV_{total} in the lumbar bone marrow significantly differed between patients who experienced disease progression during immunotherapy and those who did not. In addition, the patients with high lumbar SUV_{total} exhibited significantly lower overall survival compared with those with low vertebral signal. This finding is particularly intriguing in light of studies that suggest continuous communication between lung cancer and the bone marrow niche (32).

In patients with metastatic melanoma, a high baseline [¹⁸F]FDG signal in the bone marrow has been linked to varying clinical outcomes. One study found that an elevated [¹⁸F]FDG signal in the bone marrow indicated a favorable response to immunotherapy (33), whereas other studies reported a correlation with poor clinical outcomes (34–36). Although, in NSCLC, increased [¹⁸F]FDG metabolism in the bone marrow has been reported to inversely correlate with survival (37), in our study, we did not observe significant differences in bone marrow [¹⁸F]FDG uptake between responders and nonresponders.

Studies have reported elevated [¹⁸F]F-AraG signal in the bone marrow in both cancer patients (38) and postacute severe acute respiratory syndrome coronavirus 2 patients (39). The precise etiology of increased metabolism in the bone marrow remains elusive, despite various mechanisms having been proposed, including increased hematopoiesis (33), micrometastases (37), and systemic inflammation (35). In our preclinical studies, we observed elevated [¹⁸F]F-AraG uptake in the vertebral bone marrow in adrenergically stimulated mice as well as in mice with neuroinflammation (40). Imaging of mice deficient in T cells (*Rag1* knockout) and bone marrow adipocytes (*Letmd1* knockout) (41) after adrenergic stimulation demonstrated the crucial role of T cells in the increased [¹⁸F]F-AraG accumulation in the bone marrow. However, a comprehensive analysis of the bone marrow indicates that, in the context of adrenergic stimulation, the [¹⁸F]F-AraG signal in the lumbar bone marrow primarily originates from the tracer's uptake in metabolically active bone marrow adipocytes rather than from its accumulation in T cells (40). The ongoing studies are focused on identifying the particular mechanisms that lead to a heightened [¹⁸F]F-AraG signal in the bone marrow.

In this study, we used diagnostic [¹⁸F]FDG scans that, in some patients, were acquired close to 2 mo before the [¹⁸F]F-AraG scan. This time gap may have contributed to some of the observed differences between the [¹⁸F]FDG and [¹⁸F]F-AraG findings. To improve the accuracy of future comparisons between these 2 tracers, we will aim to acquire [¹⁸F]FDG and [¹⁸F]F-AraG scans within a 7-d window.

CONCLUSION

This study was conducted with a small number of patients, and we anticipate that the cutoff values determined in this patient group will need to be reassessed and refined in a larger patient cohort. Despite the limitations of the study size, the results underscore the significance of evaluating systemic immunity and offer initial evidence suggesting the potential of the [¹⁸F]F-AraG bone marrow signal as a predictive imaging biomarker for patient stratification and treatment guidance.

DISCLOSURE

This work was supported by National Institutes of Health Contract NCI SBIR 7575N91022C00015 (to Jelena Levi). Jelena Levi, Hilda Cabrera, and Hee-Don Chae are employed by CellSight Technologies Inc. Jelena Levi holds patents related to [¹⁸F]F-AraG. No other potential conflict of interest relevant to this article was reported.

Acknowledgments

This study is dedicated to the memory of Dr. Ananth Srinivasan, whose extraordinary intellect and boundless curiosity and enthusiasm for science profoundly impacted all who had the privilege of knowing him. We sincerely thank the patients who participated in this study for their time and commitment. We also appreciate the invaluable support of their families and medical providers.

KEY POINTS

QUESTION: Do biomarkers extracted from a preimmunotherapy [¹⁸F]F-AraG scan correlate with treatment response and overall survival in patients with NSCLC treated with anti-PD-(L)1 immunotherapy?

PERTINENT FINDINGS: In a cohort of 11 patients with advanced NSCLC, [¹⁸F]F-AraG SUV_{total} measured in the lumbar vertebrae differentiated between patients who progressed on therapy from those who did not with 90.9% accuracy. The Kaplan–Meier analysis revealed that patients with a high [¹⁸F]F-AraG SUV_{total} in the lumbar bone marrow had significantly lower probability of survival than those with a low signal.

IMPLICATIONS FOR PATIENT CARE: The results highlight the significance of systemic immunity and suggest the potential use of the [¹⁸F]F-AraG bone marrow signal as a predictive imaging biomarker for patient stratification and treatment guidance.

REFERENCES

1. Chen Z, Fillmore CM, Hammerman PS, Kim CF, Wong KK. Non-small-cell lung cancers: a heterogeneous set of diseases. *Nat Rev Cancer*. 2014;14:535–546.
2. Reck M, Remon J, Hellmann MD. First-line immunotherapy for non-small-cell lung cancer. *J Clin Oncol*. 2022;40:586–597.
3. Spigel DR, Faires-Finn C, Gray JE, et al. Five-year survival outcomes from the PACIFIC trial: durvalumab after chemoradiotherapy in stage III non-small-cell lung cancer. *J Clin Oncol*. 2022;40:1301–1311.
4. Jiménez-Sánchez A, Memon D, Pourpe S, et al. Heterogeneous tumor-immune microenvironments among differentially growing metastases in an ovarian cancer patient. *Cell*. 2017;170:927–938.e20.
5. Coley WB. II. Contribution to the knowledge of sarcoma. *Ann Surg*. 1891;14:199–220.
6. Spitzer MH, Carmi Y, Reticker-Flynn NE, et al. Systemic immunity is required for effective cancer immunotherapy. *Cell*. 2017;168:487–502.e15.

7. Gopalakrishnan V, Spencer CN, Nezi L, et al. Gut microbiome modulates response to anti-PD-1 immunotherapy in melanoma patients. *Science*. 2018;359:97–103.
8. Slebe M, Pouw JEE, Hashemi SMS, Menke-van der Houven van Oordt CW, Yaqub MM, Bahce I. Current state and upcoming opportunities for immunoPET biomarkers in lung cancer. *Lung Cancer*. 2022;169:84–93.
9. Eertink JJ, Bahce I, Waterton JC, et al. The development process of ‘fit-for-purpose’ imaging biomarkers to characterize the tumor microenvironment. *Front Med (Lausanne)*. 2024;11:1347267.
10. Kim W, Le TM, Wei L, et al. [¹⁸F]CFA as a clinically translatable probe for PET imaging of deoxycytidine kinase activity. *Proc Natl Acad Sci USA*. 2016;113:4027–4032.
11. Edwards KJ, Chang B, Babazada H, et al. Using CD69 PET imaging to monitor immunotherapy-induced immune activation. *Cancer Immunol Res*. 2022;10:1084–1094.
12. Alam IS, Mayer AT, Sagiv-Barfi I, et al. Imaging activated T cells predicts response to cancer vaccines. *J Clin Invest*. 2018;128:2569–2580.
13. Levi J, Song H. The other immuno-PET: metabolic tracers in evaluation of immune responses to immune checkpoint inhibitor therapy for solid tumors. *Front Immunol*. 2023;13:1113924.
14. Levi J, Duan H, Yaghoubi S, et al. Biodistribution of a mitochondrial metabolic tracer, [¹⁸F]F-AraG, in healthy volunteers. *Mol Imaging*. 2022;2022:3667417.
15. Levi J, Lam T, Goth SR, et al. Imaging of activated T cells as an early predictor of immune response to anti-PD-1 therapy. *Cancer Res*. 2019;79:3455–3465.
16. Levi J, Goth S, Huynh L, et al. ¹⁸F-AraG PET for CD8 profiling of tumors and assessment of immunomodulation by chemotherapy. *J Nucl Med*. 2021;62:802–807.
17. Santoro-Fernandes V, Huff D, Scarpelli ML, et al. Development and validation of a longitudinal soft-tissue metastatic lesion matching algorithm. *Phys Med Biol*. 2021;66:155017.
18. Rueckert D, Sonoda LI, Hayes C, Hill DL, Leach MO, Hawkes DJ. Nonrigid registration using free-form deformations: application to breast MR images. *IEEE Trans Med Imaging*. 1999;18:712–721.
19. Rigaud B, Simon A, Castelli J, et al. Deformable image registration for radiation therapy: principle, methods, applications and evaluation. *Acta Oncol*. 2019;58:1225–1237.
20. Huff DT, Santoro-Fernandes V, Chen S, et al. Performance of an automated registration-based method for longitudinal lesion matching and comparison to inter-reader variability. *Phys Med Biol*. 2023;68:175031.
21. Weisman AJ, Huff DT, Govindan RM, Chen S, Perk TG. Multi-organ segmentation of CT via convolutional neural network: impact of training setting and scanner manufacturer. *Biomed Phys Eng Express*. 2023;9:065021.
22. Kim SI, Cassella CR, Byrne KT. Tumor burden and immunotherapy: impact on immune infiltration and therapeutic outcomes. *Front Immunol*. 2021;11:629722.
23. Ronald JA, Kim BS, Gowrishankar G, et al. A PET imaging strategy to visualize activated T cells in acute graft-versus-host disease elicited by allogeneic hematopoietic cell transplant. *Cancer Res*. 2017;77:2893–2902.
24. Swanton C, Bernard E, Abbosh C, et al. Embracing cancer complexity: hallmarks of systemic disease. *Cell*. 2024;187:1589–1616.
25. Dall’Olio FG, Marabelle A, Caramella C, et al. Tumour burden and efficacy of immune-checkpoint inhibitors. *Nat Rev Clin Oncol*. 2022;19:75–90.
26. Evangelista L, Cuppari L, Menis J, et al. ¹⁸F-FDG PET/CT in non-small-cell lung cancer patients: a potential predictive biomarker of response to immunotherapy. *Nucl Med Commun*. 2019;40:802–807.
27. Dall’Olio FG, Calabro D, Conci N, et al. Baseline total metabolic tumour volume on 2-deoxy-2-[¹⁸F]fluoro-D-glucose positron emission tomography-computed tomography as a promising biomarker in patients with advanced non-small cell lung cancer treated with first-line pembrolizumab. *Eur J Cancer*. 2021;150:99–107.
28. Yamaguchi O, Kaira K, Hashimoto K, et al. Tumor metabolic volume by ¹⁸F-FDG-PET as a prognostic predictor of first-line pembrolizumab for NSCLC patients with PD-L1 \geq 50. *Sci Rep*. 2020;10:14990.
29. Reinfeld BI, Madden MZ, Wolf MM, et al. Cell-programmed nutrient partitioning in the tumour microenvironment. *Nature*. 2021;593:282–288.
30. Wallace DC. Mitochondria and cancer. *Nat Rev Cancer*. 2012;12:685–698.
31. Seith F, Forscher A, Weide B, et al. Is there a link between very early changes of primary and secondary lymphoid organs in ¹⁸F-FDG-PET/MRI and treatment response to checkpoint inhibitor therapy? *J Immunother Cancer*. 2020;8:e000656.
32. Calderon-Espinosa E, De Ridder K, Benoot T, et al. The crosstalk between lung cancer and the bone marrow niche fuels emergency myelopoiesis. *Front Immunol*. 2024;15:1397469.
33. Schwenck J, Schorg B, Fiz F, et al. Cancer immunotherapy is accompanied by distinct metabolic patterns in primary and secondary lymphoid organs observed by non-invasive in vivo ¹⁸F-FDG-PET. *Theranostics*. 2020;10:925–937.
34. Jeong SY, Kim SJ, Pak K, Lee SW, Ahn BC, Lee J. Prognostic value of ¹⁸F-fluorodeoxyglucose bone marrow uptake in patients with solid tumors: a meta-analysis. *Medicine (Baltimore)*. 2018;97:e12859.
35. Nakamoto R, Zaba LC, Liang T, et al. Prognostic value of bone marrow metabolism on pretreatment ¹⁸F-FDG PET/CT in patients with metastatic melanoma treated with anti-PD-1 therapy. *J Nucl Med*. 2021;62:1380–1383.
36. Seban RD, Nemer JS, Marabelle A, et al. Prognostic and theranostic ¹⁸F-FDG PET biomarkers for anti-PD1 immunotherapy in metastatic melanoma: association with outcome and transcriptomics. *Eur J Nucl Med Mol Imaging*. 2019;46:2298–2310.
37. Prévost S, Boucher L, Larivee P, Boileau R, Benard F. Bone marrow hypermetabolism on ¹⁸F-FDG PET as a survival prognostic factor in non-small cell lung cancer. *J Nucl Med*. 2006;47:559–565.
38. Wijngaarden JE, Slebe M, Pouw J, et al. Pharmacokinetic analysis and simplified uptake measures for tumour lesion [¹⁸F]F-AraG PET imaging in patients with non-small cell lung cancer. *Eur J Nucl Med Mol Imaging*. 2024; <https://doi.org/10.1007/s00259-024-06931-3>.
39. Peluso MJ, Ryder D, Flavell RR, et al. Tissue-based T cell activation and viral RNA persist for up to 2 years after SARS-CoV-2 infection. *Sci Transl Med*. 2024;16:eadk3295.
40. Levi J, Guglielmetti C, Henrich TJ, et al. [¹⁸F]F-AraG imaging reveals association between neuroinflammation and brown- and bone marrow adipose tissue. *Commun Biol*. 2024;7:793.
41. Choi KM, Kim JH, Kong X, et al. Defective brown adipose tissue thermogenesis and impaired glucose metabolism in mice lacking Letmd1. *Cell Rep*. 2021;37:110104.